

Dynamic Surface Layer Coiled Coil Proteins Processing Analog-to-Digital Information

Chiara Glionna, Vinod Kumar, Guillaume Le Saux, Bapan Pramanik, Nathaniel Wagner, Rivka Cohen-Luria, Gonen Ashkenasy,* and Nurit Ashkenasy*

Cite This: *J. Am. Chem. Soc.* 2021, 143, 17441–17451

Read Online

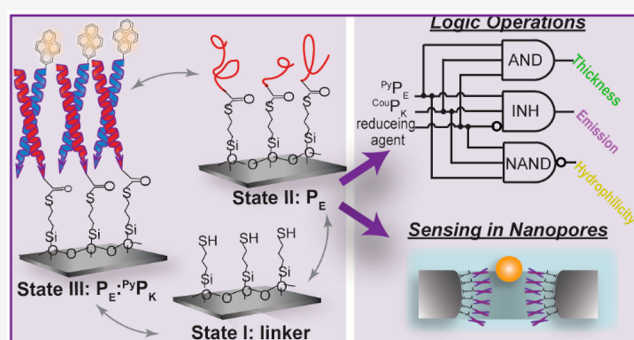
ACCESS |

Metrics & More

Article Recommendations

Supporting Information

ABSTRACT: Surface layer proteins perform multiple functions in prokaryotic cells, including cellular defense, cell-shape maintenance, and regulation of import and export of materials. However, mimicking the complex and dynamic behavior of such two-dimensional biochemical systems is challenging, and hence research has so far focused mainly on the design and manipulation of the structure and functionality of protein assemblies in solution. Motivated by the new opportunities that dynamic surface layer proteins may offer for modern technology, we herein demonstrate that immobilization of coiled coil proteins onto an inorganic surface facilitates complex behavior, manifested by reversible chemical reactions that can be rapidly monitored as digital surface readouts. Using multiple chemical triggers as inputs and several surface characteristics as outputs, we can realize reversible switching and logic gate operations that are read in parallel. Moreover, using the same coiled coil protein monolayers for derivatization of nanopores drilled into silicon nitride membranes facilitates control over ion and mass transport through the pores, thereby expanding the applicability of the dynamic coiled coil system for contemporary stochastic biosensing applications.



1. INTRODUCTION

Over the past few decades, the collective efforts of the scientific community at large have provided insight into the structural organization and structure–function relationships of countless biochemical systems. Much of this knowledge is now guiding the design of biomaterials for multiple uses in biotechnology and nanotechnology. Of particular interest, direct manipulations of native protein sequences and the *de novo* design of non-native sequences are being implemented for the development of molecules and assemblies with properties and functions that differ from—and sometimes even surpass—those of their natural counterparts.^{1–6} Investigations in this arena have traditionally targeted thermodynamically stable, “static” unimolecular architectures or small complexes. However, inspired by the dynamic nature of protein networks in cells, scientists have recently expanded the repertoire of protein functions through the preparation and characterization of relatively complex synthetic networks.^{7–11} We now show that further progress toward real-world applications can be achieved via dynamic assembly of proteins into extended arrays on solid-state surfaces, akin to a 2D monolayer. Our strategy is based on conceptually mimicking the functionality associated with the 2D layers of proteins covering the surface of prokaryotic cells, also known as s-layer proteins.^{12–16} The dynamic assembly of these natural proteins is affected by

various chemical cues (e.g., binding to calcium ions), and the resulting (para)crystalline layers, which are ~10 nm thick, serve as an additional barrier and communication platform between the cell and its environment. We show herein that the assembly/disassembly of synthetic coiled coil proteins onto a solid-state surface is controlled by multiple triggers and that the newly formed monolayers of ~8 nm thickness exhibit a variety of surface layer properties, enabling multiplex surface functionality.

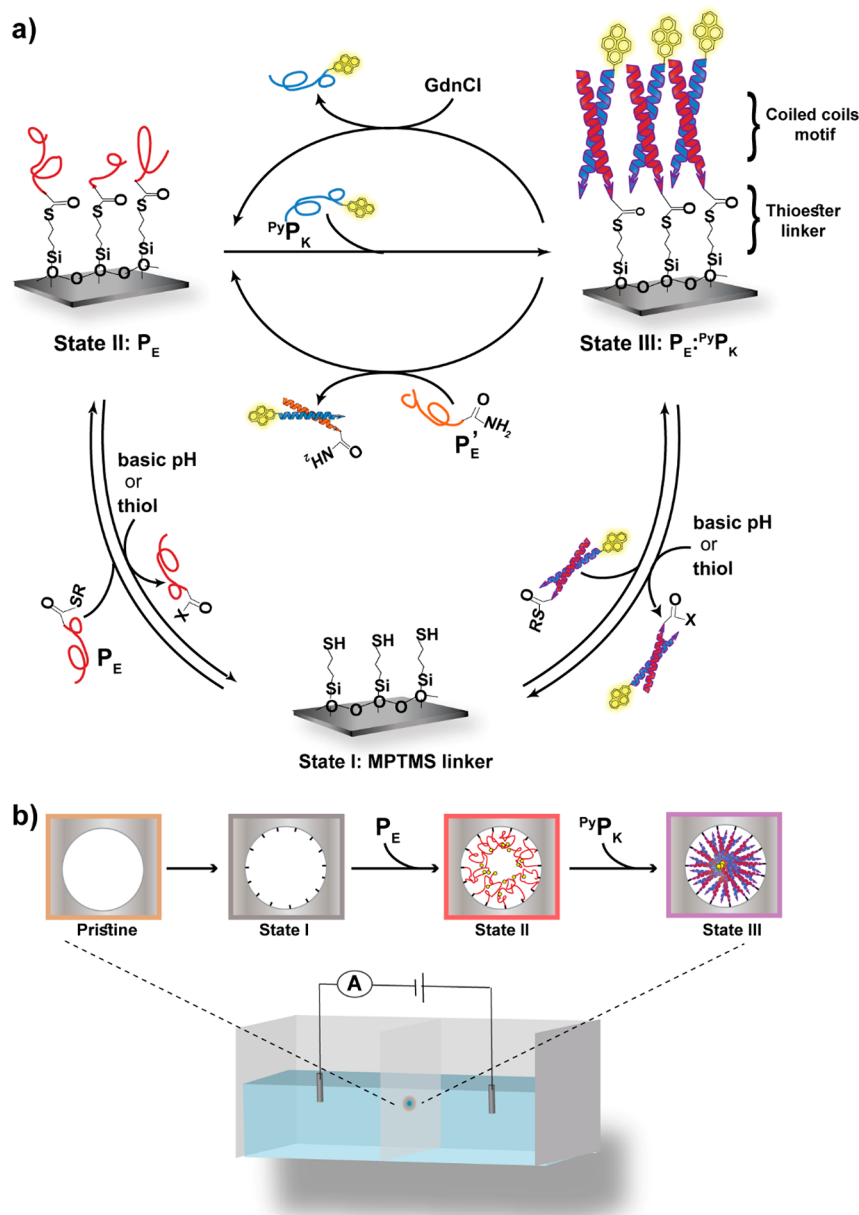
In previous work on the development of synthetic dynamic networks, it was shown that the high-density information embedded in such networks can be harnessed as Boolean logic gates and more sophisticated chemical computation schemes that produce digital outputs. The motivation for our current research originates from ample recent evidence that molecular computation can promote the development of intricate functional systems (“devices”) for delivery, sensing, molecular electronics, and more.^{17–32} On the basis of an early body of

Received: June 22, 2021

Published: October 15, 2021



Scheme 1. Dynamic Assembly of Coiled Coil Protein Monolayers: (a) Reaction Cycle Connecting the Three Monolayer States and the Different Triggers and Environmental Conditions Applied to Cause Switching between the States; (b) Representation of Nanopores in the Pristine State and after Each Step of Functionalization by the Protein Monolayers as Depicted in (a); the Nanopore Measurement Setup Is Shown at the Bottom



work that elucidated the sequence-specific oligomerization of coiled coil proteins,^{33–36} we developed, a few years ago, various logic gates and simple computational elements propelled by template-assisted autocatalysis and cross-catalysis reactions.^{37–39} Remarkably, related coiled coil protein systems have very recently facilitated modular protein logic for regulating functions in cells.^{40–43} However, the utility of these systems has been largely limited to soluble monomeric proteins or small complexes. We postulated that exploiting dynamic protein assemblies on surfaces will allow expanding the repertoire of accessible logic operations, facilitate easier detection of the gate outputs, and may open the way for multiple uses of the protein-derivatized surfaces, for example in sensing applications.

A small number of studies, including a work by the authors,⁴⁴ have demonstrated in the past coiled coils assembly on gold surfaces^{45–48} and have furthermore revealed that the specific interactions between the peptide helices forming the proteins can be utilized to control the aggregation of gold nanoparticles^{47,48} or the electronic properties of the surfaces on which they assembled and controlled charge transport to the surface.⁴⁴ In the current work, we address the next mechanistic challenge by presenting a dynamic system that operates reversibly on a silicon nitride (Si_3N_4) surface, turning it into a responsive functional system. Triggering the interconversion between coiled coil protein monolayer states leads to changes in several Si_3N_4 surface characteristics, including its dielectric response, hydrophobicity, and light emission properties. We exploit these changes as the digital

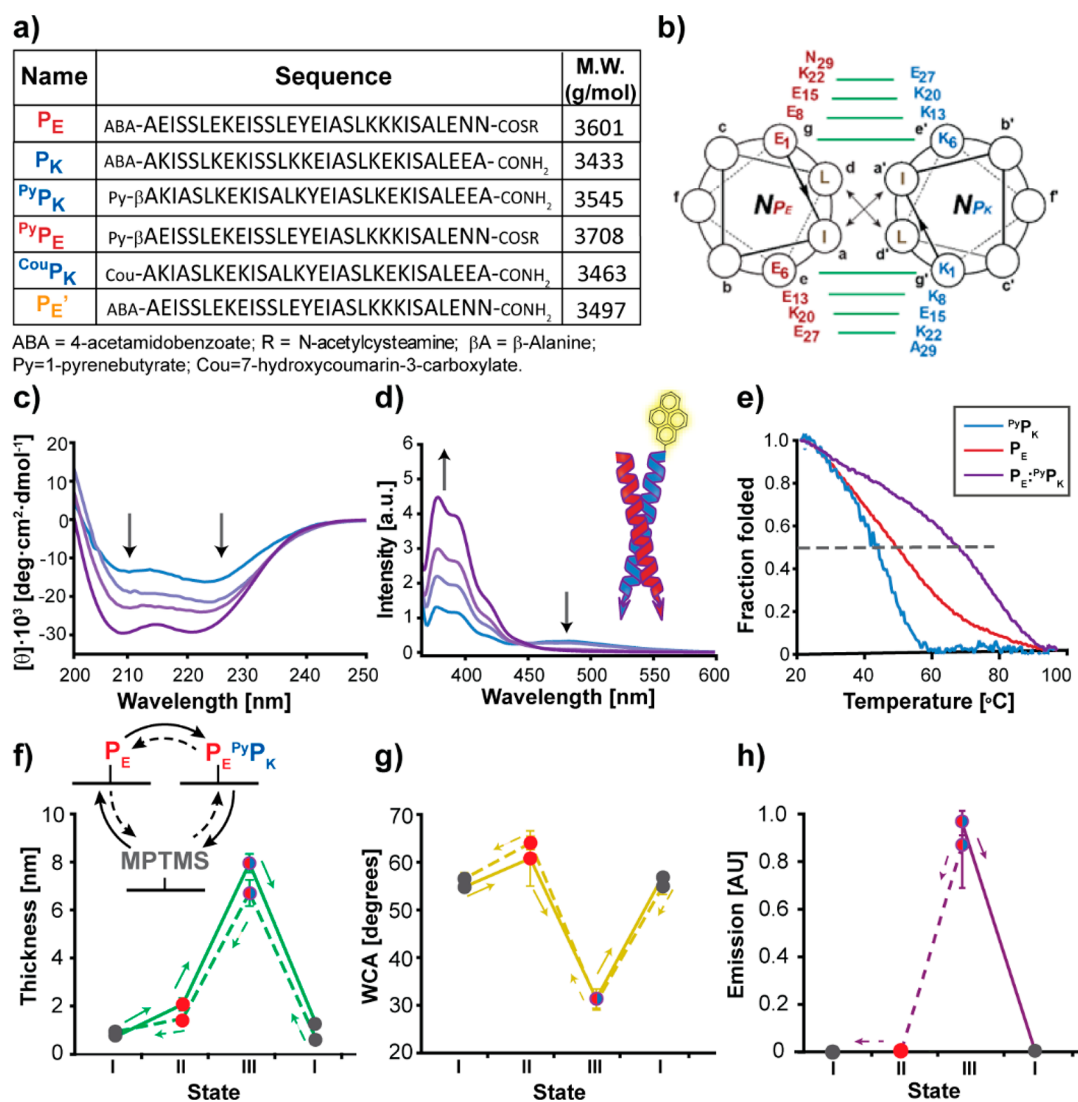


Figure 1. (a) Peptide sequences used in this study and their measured molecular weights. (b) Helical wheel representation of the glutamic acid-rich (P_E) and lysine-rich (P_K) peptides forming the heterodimeric parallel coiled coil assemblies. (c–e) Structural characterization of the heterodimeric coiled coil complexes in solution. (c) Circular dichroism (CD) characterization of P_E : PyP_K complex formation during the titration of a PyP_K solution (17.5 μ M) with a P_E solution (0, 4, 8, and 17.5 μ M; shown as the shift from the blue to purple plots). (d) Fluorescence spectra ($\lambda_{ex} = 344$ nm) obtained for the titrated samples shown in (c). (e) Helically folded fractions as a function of the temperature, deduced from the (222 nm) CD signals during thermal denaturation of P_E (35 μ M), PyP_K (35 μ M), or P_E : PyP_K (17.5 μ M each). Experiments in (c–e) were performed in 5 mM MOPS buffer, pH 7. (f–h) Surface characterizations during the reaction cycle depicted in the inset to (f). Switching in the clockwise (solid line) or anticlockwise (dashed line) directions is presented by changes in the surface complex refractive index (f) measured by ellipsometry and presented as monolayer thickness, in the water contact angle (WCA) in (g) and in the fluorescence emission (h; $\lambda_{ex} = 342$ nm, $\lambda_{em} = 386$ nm).

outputs of chemical switches and logic gates. Remarkably, we demonstrate that multiple gates can be operated simultaneously in a single process. To demonstrate the applicability of the new system, we show that the output of the digital switches and logic gates can be read directly as an electronic signal by using the protein monolayers to modulate the ion current through nanopores drilled into a Si_3N_4 membrane. This setup is utilized here to affect and amplify the signal signature of an analyte translocation through the nanopores, thus making our system attractive for future stochastic sensing applications.^{49–51}

2. RESULTS AND DISCUSSION

2.1. Dynamic Coiled Coil Protein Monolayer Reaction Cycle.

We utilized coiled coil proteins containing short thioester linkers to prepare dynamic monolayers on Si_3N_4

surfaces or at the rims of nanometric pores drilled in Si_3N_4 -based membrane devices (Scheme 1). The coiled coil structural motif is frequently found in native proteins (appears in >5% of all protein structures),³⁵ and the design constraints on coiled coil folding have been clearly identified.^{4,35,52–58} We hypothesized that the high modularity of the coiled coil system and its responsiveness to multiple external triggers allow the design of dynamic protein layers on a solid support. In our system, glutamic acid-rich (P_E) and lysine-rich (P_K) peptide sequences were designed such that they would form parallel heterodimeric complexes of about 7 kDa, containing a Ile-Leu hydrophobic core and exhibiting perfect charge matching between residues at the g and e heptad positions of the opposing helices (Figure 1a,b).^{36,44} The C-terminus of P_E was functionalized with a short thioester group to allow dynamic covalent attachment to a thiol-bearing Si_3N_4 surface. This

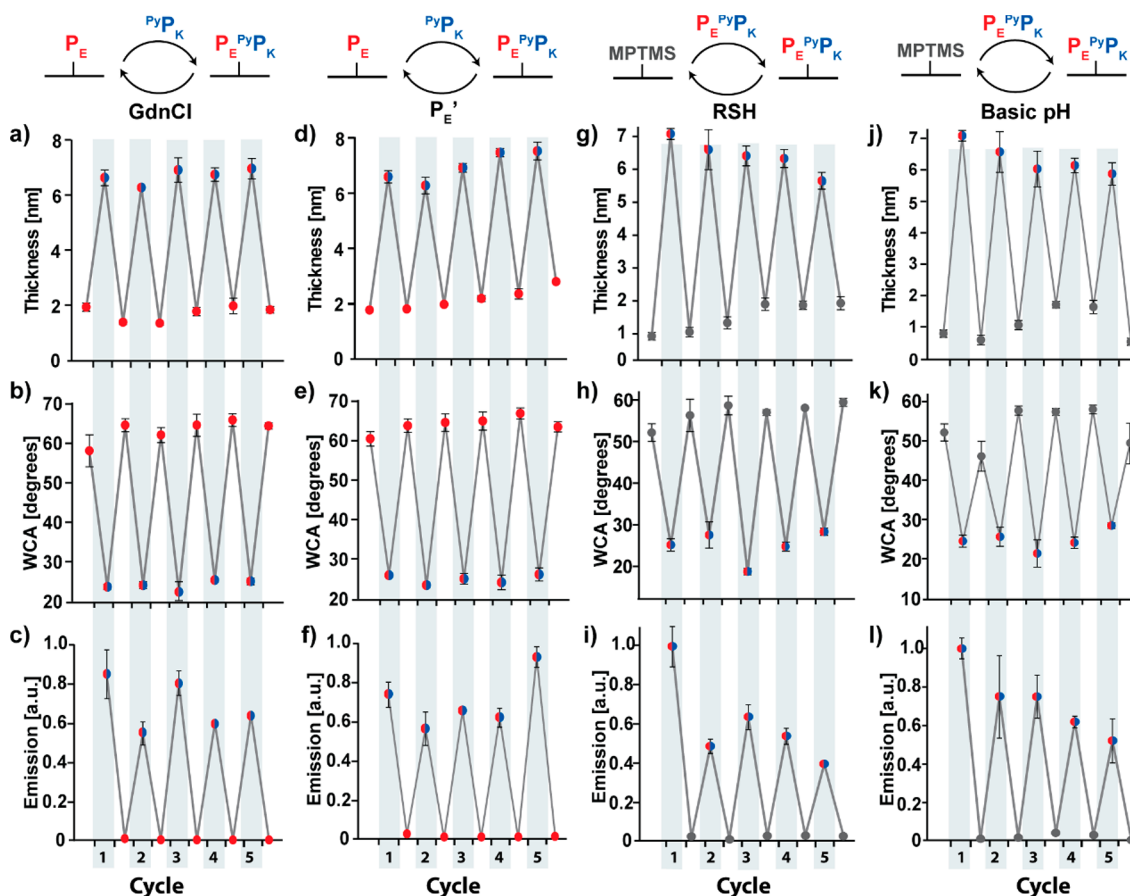


Figure 2. Dynamic switching between surface monolayer states. (a–f) Changes in surface characteristics (layer thickness, water contact angle, and 386 nm light emission) observed during five switching cycles between monolayer state II and state III. Switching from state II to III was induced by the assembly of ${}^{\text{Py}}\text{P}_{\text{K}}$ on P_{E} -functionalized Si_3N_4 surfaces. Switching back to state II was obtained by denaturation with GdnCl (a–c) or by adding the competitor molecule P_{E}' (d–f). (g–l) Changes in surface characteristics observed during five switching cycles between state I and state III. Switching from state I to state III was induced by the assembly of the $\text{P}_{\text{E}}:{}^{\text{Py}}\text{P}_{\text{K}}$ coiled coil complex on MPTMS-functionalized Si_3N_4 surfaces; switching back to state I was obtained via the TTE reaction (using SNAC = RSH; (g–i)) or hydrolysis at pH 8 (j–l). Specific reaction conditions are given in the [Supporting Information](#), section 1.3.

reversible covalent bonding, together with the assembly/disassembly process of the coiled coils, enabled active triggering and interconversion between three different monolayers: 3-mercaptopropyltrimethoxysilane (MPTMS) linkers, termed state I, peptide monomers (P_{E}), state II, and folded coiled coil heterodimers ($\text{P}_{\text{E}}:{}^{\text{Py}}\text{P}_{\text{K}}$), state III (Scheme 1a). Various chemical triggers, namely, pH regulation and/or the introduction of small molecules or competing peptide molecules, were used to reversibly activate the switching from one assembly state to another (Scheme 1).

All P_{E} and P_{K} peptide derivatives (Figure 1a) were synthesized and purified in-house and characterized by HPLC and MS (Figures S1 and S2). The P_{K} and/or P_{E} N-termini were equipped with pyrene or coumarin dyes (Figure 1a), when needed, providing light emission tags to detect changes in direct fluorescence or Förster resonance energy transfer (FRET). Titration assays performed by the addition of increasing amounts of P_{E} into ${}^{\text{Py}}\text{P}_{\text{K}}$ solutions revealed the exclusive formation of heterodimeric coiled coil complexes, as shown by the appearance of the typical coiled coil helix circular dichroism (CD) signal (Figure 1c) and an increase in pyrene monomer fluorescence emission associated with the disassembly of the weakly held ${}^{\text{Py}}\text{P}_{\text{K}}$ dimers (Figure 1d). In addition, thermal denaturation experiments (Figure 1e)

showed that the heterodimeric coiled coils complex with melting temperature $T_{\text{m}} = 68$ °C was significantly more stable than the respective homodimeric complexes ($T_{\text{m}} = 49.5$ °C and $T_{\text{m}} = 42$ °C for P_{E} and ${}^{\text{Py}}\text{P}_{\text{K}}$ dimers, respectively).

We established a fully reversible interconversion between protein assembly states by switching in two opposite reaction pathways: state I \rightarrow II \rightarrow III \rightarrow I and state I \rightarrow III \rightarrow II \rightarrow I (Scheme 1 and Figure 1f–h). Three different surface properties, i.e., the complex refractive index as measured by ellipsometry and presented as the layer thickness (Figure 1f), wettability, expressed as the water contact angle (WCA; Figure 1g), and fluorescence emission (Figure 1h), were affected by the transition between the monolayer states and were monitored in parallel.

Switching from state I to state II was readily achieved by exposing the MPTMS monolayer to the P_{E} solution (0.75 mM, overnight) and yielded an increase of about 1 nm in the layer thickness (Figure 1f), suggesting that the P_{E} monolayer was organized in a partially collapsed random coil conformation. This molecular arrangement could also explain the moderate change in surface hydrophobicity (Figure 1g), inferred from the WCA measurements, upon transition from state I ($\theta \approx 57^\circ$) to state II ($\theta \approx 64^\circ$). State II was triggered to switch into state III by exposing the P_{E} monolayer to a ${}^{\text{Py}}\text{P}_{\text{K}}$ peptide

solution (0.18 mM; 1 h), forming a monolayer of the folded coiled coil complex ($P_E \cdot P_K$). Following this process, we observed a significant increase of 6.1 ± 0.5 nm in layer thickness (Figure 1f), which is of the same order as the full length of 6.7 nm of the coiled coils assembly in solution,^{44,59} thus implying a nearly vertical configuration and high coverage of the surface by the proteins. A significantly more hydrophilic surface was obtained for state III ($\theta \approx 25^\circ$; Figure 1g), indicating that the hydrophobic amino acids of the coiled coil complexes were buried in the assembly core, while the hydrophilic side chains remained accessible to the aqueous environment. Additionally, the surface layer fluorescence emission (386 nm), which was low in the absence of dyes (states I and II), increased significantly upon adsorption of the fluorescently tagged P_K molecules in state III (Figure 1h). To complete this cycle, state III was switched to state I by hydrolysis of the thioester bond in an alkaline environment (pH 8; 1.5 h twice), yielding significant reductions in the layer thickness and surface emission and an increase in the WCA (Figure 1f–h).

In the reverse process, state III was directly prepared from state I by exposing the MPTMS-functionalized surface to a solution of premade coiled coil $P_E \cdot P_K$ protein (0.18 mM; 1 h). Previous studies have demonstrated the coiled coil monolayers disassembly through denaturation due to pH and/or temperature changes.^{46,47} Here, denaturation by adding the guanidine hydrochloride denaturant (GdnCl; 6 M; 1 h) led to switching state III back to state II. The process again led to reductions in the layer thickness and the fluorescence signal and an increase in the WCA to give values representative of state II (Figure 1f–h). Finally, state II was switched back to state I by alkaline hydrolysis of the thioester bond, leading to a further reduction in layer thickness and an increase in the WCA (Figure 1f–h). Notably, all three surface properties remained almost the same after completing the reaction cycles, regardless of the pathway direction (Figure 1f–h).

2.2. Reversible Switching of the Surface-Layer Protein Properties. An important bioinspired feature of our new system is that multiple triggers could be applied for switching between the different states (Scheme 1). For example, switching state III to state II could be achieved either by adding GdnCl (Figure 1f–h) or by introducing a competitor peptide, P_E' —identical in sequence to P_E but lacking the C-terminus thioester group—to hybridize with P_K , thereby removing it from the surface (Scheme 1 and Figure 1a). Likewise, switching from state II to state I (or from state III to state I) could be performed by alkaline hydrolysis (Figure 1f–h) or by a trans-thioesterification (TTE) reaction induced by the addition of a small thiol molecule (*N*-acetylcysteamine; SNAC; 3 mM, 1.5 h three times). Furthermore, the reversible nature of the system allowed us to repeatedly switch between the three states, enabling parallel changes in the layer thickness, wettability, and emission surface characteristics (Figure 2). Five successive cycles of switching between monolayer states II and III were completed by inducing the folding and assembly of coiled coil protein monolayers, via the addition of the P_K monomer to surfaces prefunctionalized with the P_E peptide, and triggering the reverse coiled coil unfolding process by either (GdnCl) denaturation (Figure 2a–c) or competition with P_E' (0.4 mM; 1 h) (Figure 2d–f). Repetitive switching between monolayer states I and III was achieved by the direct assembly of the $P_E \cdot P_K$ complex on MPTMS-functionalized surfaces

and its detachment via either a TTE reaction (Figure 2g–i) or hydrolysis of the thioester bond at pH 8 (Figure 2j–l). These multiple switching patterns confirmed, once again, the fully reversible nature of the assembly processes needed to facilitate the gating functions discussed in the following sections. A slight degradation of the coiled coils monolayer (state III in Figures 2g–i and 2j–l) was observed during continuous cycling. We attribute this degradation to partial prevention of the coiled coil formation by nonspecifically attached protein molecules remaining from previous cycles.

The dynamic assembly of the protein monolayers was then used to control the ion flow through nanopores functionalized with the coiled coil proteins (Scheme 1b). The nanopore ion current, which depends to a significant extent on the nanopore effective diameter and the chemophysical properties of its rim, has often been used as a detection signal in biosensing devices.^{60–62} Following our previous demonstration that fluctuations in the nanopore ion current can be used to monitor minute changes in the folding state of a peptide monolayer,⁶³ we postulated that the changes in the coiled coil monolayer states, which are accompanied by changes in the layer thickness (Figure 1f), could be followed by monitoring the current. The ohmic current–voltage (I – V) relationship was monitored first for the pristine nanopore (about 14 nm in diameter) and after functionalization of the nanopore rim with MPTMS, P_E , and $P_E \cdot P_K$ (states I, II, and III, respectively). The resultant reduction in the ionic current with each functionalization step (Figure 3a) signified a reduction in the effective diameter of the nanopore, which was evaluated by using the simple relationship $d = \sqrt{\frac{4GL}{\sigma\pi}}$, where d is the effective pore diameter, G the conductance of the nanopore, L the thickness (20 nm) of the membrane, and σ the solution conductivity (10.5 S m^{-1} at 23 °C).⁶⁴ Accordingly, the effective thickness of the functionalizing layer t_{ML} was calculated as $t_{ML} = (d_{\text{pristine}} - d_{\text{state } i})/2$, where d_{pristine} and $d_{\text{state } i}$ are the pristine and functionalized nanopore diameters, respectively. Excellent agreement was found between the layer thickness calculated from the nanopore conductivity and ellipsometry measurements of samples prepared on silicon nitride submerged in parallel in the electrolyte cell (Figure 3b). Covering the nanopore with the coiled coil assemblies (state III) induced an almost complete shuttering of the pore (>90% blockade), indicating that the respective monolayer thickness values account for the formation of highly dense monolayers. Considering that a single coiled coil complex occupies an area of $\sim 200 \text{ \AA}^2$,⁴⁴ we calculated that the state III coiled coil monolayer consisted of about 900 protein dimer assemblies within the nanopore.

Switching between the partially open state II and the almost completely blocked state III of the silicon nitride nanopores was achieved by *in situ* alternating additions of P_K (state II \rightarrow III) and GdnCl (state III \rightarrow II) to the electrolyte solutions (Figure 3c). Indeed, the current flowing through the nanopore decreased and increased consecutively, as reflected by the percent blockage, calculated as the percentage of residual current with respect to the current flowing through the pristine nanopore (Figure 3c). The switching process was found to be extremely robust for at least five cycles. Here again, the changes in the thickness of the functionalizing layer on the nanopore rim, calculated from the measured I – V values, were very similar to the values obtained from ellipsometry on silicon nitride chips immersed in the measurement cell (Figure S3).

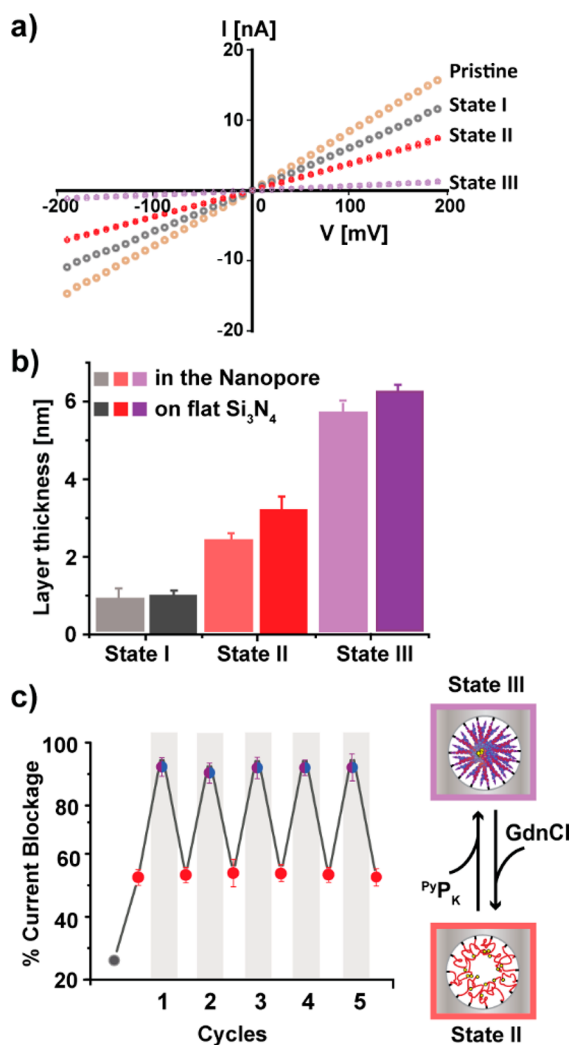


Figure 3. Gating silicon nitride nanopores with the coiled coil protein monolayers. (a) I – V relations for the pristine nanopore (14 nm commercial nanopore in a 20 nm thick silicon nitride membrane) and after functionalizing the nanopore rim with MPTMS (state I), P_E (state II), and $\text{P}_E:\text{P}_K$ (state III) monolayers. Curves were measured from -190 to $+190$ mV with 10 mV intervals of 0.25 s each for nanopore membranes sandwiched between two reservoirs of a Teflon cell filled with KCl solution (1 M) in Tris-HCl buffer (10 mM, pH 7) and equipped with Ag/AgCl electrodes (see Scheme 1b). (b) Comparison of the layer thicknesses calculated from the ellipsometry measurements and from the nanopore conductance values (slopes of the I – V curves in panel a). (c) Sequential reversible nanopore gating by continuous *in situ* switching between states II and III. The current blockage (%) in each cycle was calculated from the current changes $\Delta I/I$, where I is the current at 190 mV of the pristine nanopore and ΔI is the difference between this value and the current measured for the functionalized nanopore under the same applied bias.

2.3. Computational Logic Gate Motifs in the Dynamic Coiled Coil Surface Layers. The high-density molecular information contained within the coiled coil dynamic system (Figures 1 and 2) was exploited to express several Boolean logic gates and simple computation operations. To expand the array of digital signals available to produce the gates, two slightly modified peptides were synthesized as a FRET pair, namely, the thioester peptide PyP_E (a P_E sequence labeled with a pyrene moiety) as the FRET donor and the complementary peptide CouP_K (P_K labeled with 7-hydroxycoumarin) as the

FRET acceptor (sequences are shown in Figure 1a). Titration experiments, performed by the gradual addition of a CouP_K solution into a PyP_E solution, showed a gradual reduction in pyrene monomer emission (~ 390 nm) and in the excimer emission (~ 490 nm) associated with the disassembly of the weakly held PyP_E dimer, accompanied by an increase of the FRET emission at 455 nm due to the formation of the $\text{PyP}_E:\text{CouP}_K$ complex (Figure 4a).

As a first demonstration, the NOR and OR logic gates were realized in parallel by using the monolayer of heterodimer $\text{PyP}_E:\text{CouP}_K$ coiled coil complex (state III) as the initial gate state and the competitor peptide P_E' and GdnCl as the gate inputs (Figure 4b). As could be expected from the similarity in monolayer characteristics for $\text{PyP}_E:\text{CouP}_K$ and the above-discussed $\text{P}_E:\text{PyP}_K$ complex, state III (0,0 input) comprised a thick monolayer (~ 6 nm; Figure S4a) of folded proteins. This arrangement has brought the FRET dyes of PyP_E and CouP_K close to each other, hence emitting light at ~ 450 nm (Figure S4b). Introducing either one of the two gate inputs separately, or both together, triggered unfolding of the coiled coil assembly and the release of CouP_K , leaving behind a monolayer of the random coil PyP_E molecules. Therefore, the surface layer thickness measurements indicated a decrease for each one of the latter input combinations to ~ 2 nm (Figure S4a), very similar to the values obtained for the P_E -modified surfaces in the above-described switching experiments (Figure 2a,d), hence accounting for the NOR gate (1000; Figure 4b). Concurrently, the fluorescence signal extracted from these input combinations as the ratio of the fluorescence emission $I_{455} = 386 \text{ nm}/I_{450} = 450 \text{ nm}$ increased due to a decrease in FRET emission at 450 nm and an increase in the pyrene monomer emission at 386 nm (Figure S4b). We note a maximal change in the FRET ratio for the (1,1) input case and slightly more modest changes for the (1,0) and (0,1) inputs, thus representing the OR function (0111; Figure 4b).

Additional demonstration for gathering the chemical information by logic operations was devised in a stepwise manner to develop a relatively complex three-input three-output gate system. In the first step, only the parallel AND and INHIBIT logic operations were accomplished by using the MPTMS-functionalized surface (state I) as the initial state, the two peptides PyP_E and CouP_K as inputs, and the surface layer thickness and fluorescence (386 nm) as parallel output signals (Figure S5). The surface thickness was found, as expected, to be low in all cases (1 and 2 nm for the MPTMS-derivatized and PyP_E -derivatized surfaces, respectively), except for the (1,1) input case when both PyP_E and CouP_K were added (sequentially) and formed a thicker layer of folded proteins (~ 6 nm; Figure S5a), thus presenting the expected AND function (0001; Figure S5c). The layer emission, measured in parallel (Figure S5b), was low when no protein was attached to the surface (0,0 input) or when CouP_K was introduced to either an MPTMS-derivatized (0,1) or a PyP_E -derivatized (1,1) surface. Almost 1 order of magnitude higher emission was observed in the case in which PyP_E alone was attached to the surface (1,0 input), reflecting the conditional INHIBIT gate (0100; Figure S5c). This experiment was a subset of a more sophisticated three-input three-logic-gates system, presenting in parallel the AND, INHIBIT, and NAND operations (Figure 4c and Figure S6). The experiment was initiated with an oxidized (disulfide) MPTMS-functionalized surface (0,0,0) state, and the third input of the logic system was the reducing agent, tris(2-carboxyethyl)phosphine (TCEP), which served to

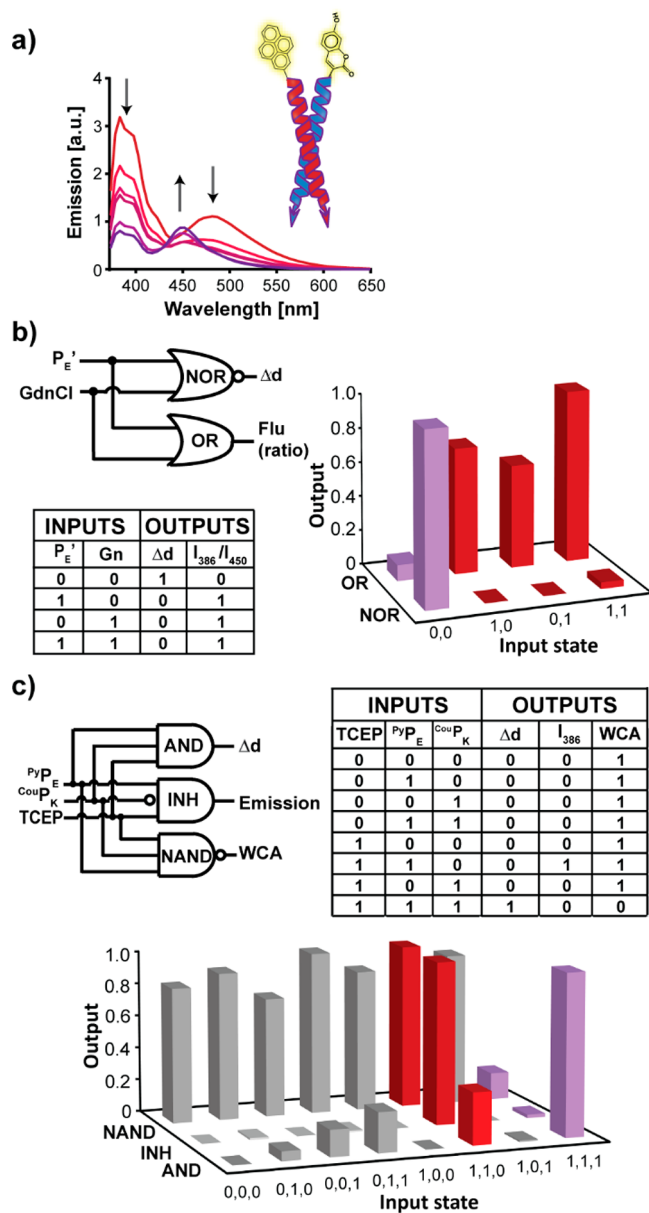


Figure 4. Expression of Boolean logic operations by using the dynamic protein surfaces. (a) Fluorescence spectra obtained for titration of a PyP_E solution (17.5 μ M) with a $CouP_K$ solution (0, 4, 8, and 17.5 μ M; shown by the shift from the red to purple plots); λ_{ex} = 342 nm. Experiments performed in 5 mM MOPS buffer pH 7.0. (b) Reaction diagram, truth tables, and experimental results for simultaneous NOR and OR gates, performed by conditional switching from state III to II by using the competitor peptide P_E' and GdnCl as orthogonal inputs. The thickness outputs of the NOR gate were normalized with respect to the (0,0) state output signal (=1.0). The emission signals of the OR gate were extracted as the ratio of the fluorescence emission $I_{\lambda} = 386 \text{ nm}/I_{\lambda} = 450 \text{ nm}$ and normalized with respect to the emission of the gate (1,1) state (=1.0). Raw experimental results are shown in Figure S4. (c) Reaction diagram, truth tables, and experimental results of the 3-input AND, INHIBIT, and NAND gates, performed by switching from state I (MPTMS monolayer) to state II or III of the dynamic system. The inputs of these gates were TCEP, PyP_E , and $CouP_K$ and the gate readouts were the layer thickness (AND; normalized for (1,1,1) output signal = 1.0), 386 nm emission intensity (INHIBIT; (1,1,0) output signal = 1.0), and the water contact angle (NAND; (1,1,0) output signal = 1.0). Raw experimental results are shown in Figure S6.

control the redox state and the availability of free MPTMS thiol head groups in state I, thereby facilitating or inhibiting the PyP_E assembly. By monitoring all three surface signals in parallel, namely, the layer thickness (Figure S6a), fluorescence (386 nm emission; Figure S6b), and hydrophobicity (WCA; Figure S6c) for the eight combinations of the three inputs, the AND (0000001), INHIBIT (00000100), and NAND (1111110) gates were successfully demonstrated (Figure 4c).

The successful design of the logic gates shown in Figure 4, particularly the parallel three-input three-output gate system, demonstrates the versatility of our dynamic assemblies in producing digital functions. We applied similar design principles to perform two independent Boolean gates using the nanopore ion current as the “1” and “0” outputs of the gates, related to the open and closed states of the nanopore, respectively. To the best of our knowledge, we present here the first demonstration of logic gate operations in nanopores driven by controlling the proteins’ folding state.

The (almost completely) open nanopore derivatized with MPTMS (state I) was the initial state, and P_E and P_K served as the inputs producing the NAND gate (Figure 5a). Here, introducing P_E (1,0) or P_K (0,1) solutions separately either did not change the current or induced only a slight decrease in the current (Figure S7a), featuring the “1” output, while the

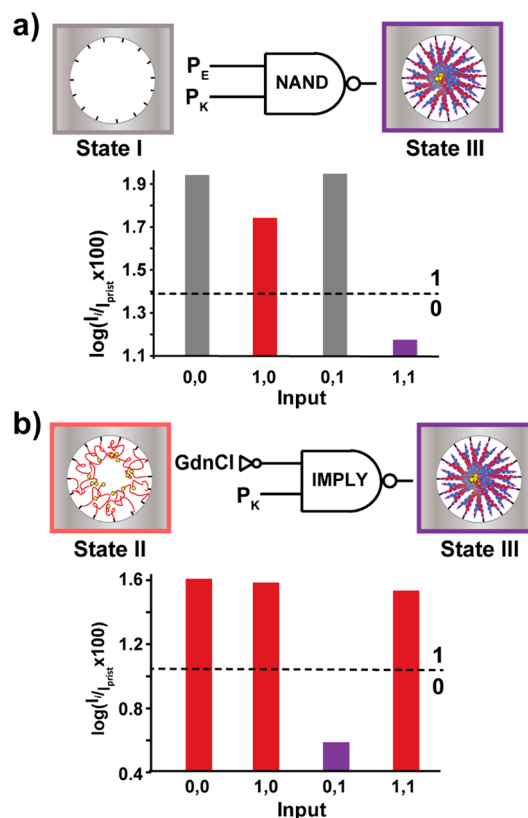


Figure 5. Expressing Boolean logic operations by nanopore gating. (a) Schematic design and experimental results displaying the NAND gate for nanopores derivatized with MPTMS (state I) as the initial state and P_E and P_K as inputs. (b) Schematic design and experimental results displaying the conditional IMPLY gate, initiating from the P_E -derivatized nanopore (state II) and using P_K and GdnCl as inputs. In all cases, “0” and “1” outputs were related to the impeded and enhanced ion current through the pores, at 190 mV, respectively. The corresponding I – V curves are presented in Figure S7.

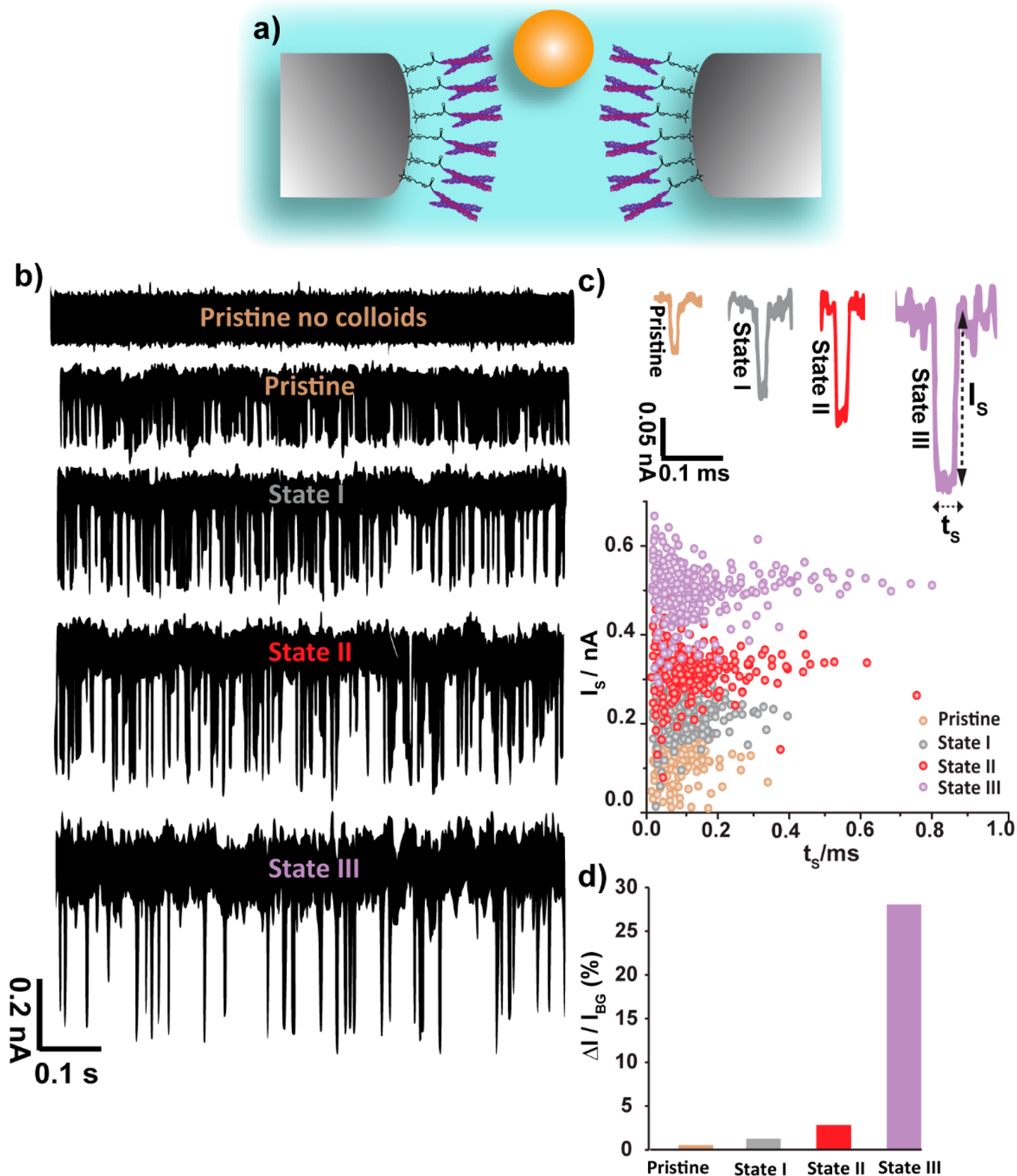


Figure 6. Amplification of the analyte translocation signal by nanopore modification with the coiled coil proteins. (a) Schematic representation of a gold colloid translocation through a nanopore modified with a coiled coils monolayer. (b) Current transient at 300 mV applied voltage for an 18 nm nanopore, modified with each one of the monolayer states, after addition of 5 nm gold colloidal particles (50 μL , 0.01%) to the *cis* chamber. Transient of the pristine nanopore before the addition of gold colloidal particles is presented at the top as a reference. Spikes in the transient plot represent current blockage due to translocation of a single gold colloidal particle through the nanopore. (c) Magnification of a typical translation spike and the corresponding spiking events' scatter graph for each of the system's states. Additional statistical analyses of the characteristics of the events are presented in Figure S9. (d) Average current blockage ($\Delta I / I_{BG}$ percentage) observed due to translocation of gold colloidal particles in each of the system states, highlighting the signal amplification factors (see text).

addition of the preassembled $P_E:P_K$ complex (1,1) significantly blocked ion transport (Figure S7a), thereby producing the “0” output signal (Figure 5a).

In a different experimental configuration, the partially open nanopore, functionalized with P_E (state II), was utilized as the initial state (0,0 input), and P_K and GdnCl solutions were introduced as inputs producing the conditional IMPLY gate (Figure 5b and Figure S7b).^{32,65} In this experiment, GdnCl served as an input (1,0 input) retaining the “1” output (state II). The system was then operated toward the production of state III by introducing P_K (0,1 input), yielding a significant current decrease as a “0” signal. However, in an experiment performed with the addition of both P_K and GdnCl (1,1 input), the latter input served predominantly as an inhibitor of the folding of the coiled coils on the nanopore rim, leaving the pore (partially) open to ion transport (state II), thus imposing a NOT function and the IMPLY gate “1” signal.

2.4. Nanopore Stochastic Sensing Amplification by the Dynamic Protein Assembly. The nanopore logic gate operations demonstrated in the previous section somewhat resemble the complex gating regulation of natural nanopores, e.g., in the nuclear pore complex.⁶⁶ In these natural nanopores, the gating is used to control mass transport between the nucleus and the cytoplasm.

In artificial silicon nitride nanopores, the translocation of molecules, which translates into spiking events in the nanopore current, has been extensively studied and was demonstrated to be useful for real life applications.^{60–62} The translocation event characteristics, which determine the sensitivity of the detection, are related to the relative current blockade during translocation and the translocation duration, which, in turn, depend on the dimensions and the surface characteristics of both the analyte and the nanopore. To test the effect of the dynamic coiled coil functionalization on analyte translocation, we monitored the temporal spiking events obtained during translocations of 5 nm gold colloidal particles, as model analytes, from the *cis* to the *trans* side of a membrane through a nanopore ~18 nm in diameter. This has emphasized that the tunability in size, offered by the peptide-functionalized nanopore, allows for pronounced amplification of the current spiking amplitude and hence improves the analyte detection signal (Figure 6).

The translocation experiments were repeated after successive modifications of the nanopore with MPTMS, P_E , and the folded $P_E:P_K$ coiled coil monolayers (states I, II, and III, respectively; Figure 6b and Figure S8). While in contrast to the natural nuclear pore complex the rate of the translocations was still significant, even for the largely shuttered nanopores state III (Figure 6b), a clear increase in the magnitude of the spike, ΔI , and its dwell time, t_s , was observed with each modification step (Figure 6b,c and Figure S9), making this platform an attractive tool for the development of sensitive biosensors. Furthermore, since ΔI increased while the background current (I_{BG}) decreased with each modification step, the absolute sensing signal, $\Delta I/I_{BG}$, increased with each modification step (Figure 6d). In particular, the first two modification steps, with MPTMS and P_E , led to an ~2-fold amplification of the signal versus the previous step, and the last modification step with the folded coiled coil $P_E:P_K$ protein led to a remarkable 1 order of magnitude additional amplification of the signal (Figure 6d). As a result, we observed an overall ~50-fold amplification between the pristine and protein modified nanopore signals. We propose that this significant amplification process, which

increases the sensitivity of the nanopore, may improve the detection of various analytes, particularly small-sized analytes. Clearly, the use of the coiled coil system allows for the fine-tuning of the nanopore diameter and surface chemistry to further improve its sensing capabilities. Furthermore, by *in situ* triggering transfer from one state of the nanopore to another, the sensitivity can be tuned reversibly during the sensing experiments, allowing for the detection of multiple analytes with a single nanopore.

3. CONCLUSIONS

Our work presents a novel surface functionalization scheme based on the reversible conversion between monolayers of coiled coil proteins and their monomeric precursors. As observed for natural s-layer proteins,^{12,16} the synthetic monolayer assembly process is affected by multiple triggers and yields changes in several surface properties simultaneously.

The novel design, affording dynamic interactions between the protein monomers, and between the proteins and the solid-state surfaces, allowed us to produce the core features of logic operations, i.e., the flow of information from one or several inputs, through a processing component to produce an output. Such behaviors have been suggested to enable sophisticated hydrogel manipulation algorithms and the development of programmable materials.⁶⁷ The conceptual logic operations implemented here included the most basic features (reversible association) and the production of multiple logic gates. Moreover, the unique properties of the design allowed for processing several operations simultaneously, producing multiple readouts in parallel. All the operations were obtained on reactive surfaces, a chemical functionality only rarely demonstrated to date,^{25,31} providing simple and fast readouts, with the “write and erase” functionality of the coiled coils system, enhancing the applicability of the design.

The applicability of our design was illustrated by using it for solid state nanopore derivatization, allowing direct electronic outputs of the logic gates to be extracted via the monitoring of ion currents through the nanopores. Moreover, in the context of stochastic sensing, the derivatization of the nanopore generated a remarkable signal amplification (up to 50-fold) for a model analyte. The ability to infer on the coiled coil state through molecular translocation characteristics, and hence on the presence of multiple stimuli for its folding/unfolding, may open the way for “one pot” detection of multiple constituents in complex media.

Our study shows that the novel *de novo* designed coiled coils monolayer system retains the complexity and dynamic behavior native to biological condensed networks and thereby offers the sophistication required to develop smart programmable materials and surfaces as well as advanced sensing schemes.

■ ASSOCIATED CONTENT

Supporting Information

The Supporting Information is available free of charge at <https://pubs.acs.org/doi/10.1021/jacs.1c06356>.

Experimental details, peptides' characterization data, row data of Boolean gates expression experiments on surface and in nanopore, additional data of gold colloids translocation experiments (PDF)

AUTHOR INFORMATION

Corresponding Authors

Gonen Ashkenasy – Department of Chemistry and Ilse Katz Institute for Nanoscale Science and Technology, Ben-Gurion University of the Negev, Beer-Sheva 84105, Israel; Email: gonenash@bgu.ac.il

Nurit Ashkenasy – Department of Materials Engineering and Ilse Katz Institute for Nanoscale Science and Technology, Ben-Gurion University of the Negev, Beer-Sheva 84105, Israel; orcid.org/0000-0003-2880-9293; Email: nurita@bgu.ac.il

Authors

Chiara Glionna – Department of Chemistry, Ben-Gurion University of the Negev, Beer-Sheva 84105, Israel

Vinod Kumar – Department of Materials Engineering, Ben-Gurion University of the Negev, Beer-Sheva 84105, Israel

Guillaume Le Saux – Department of Materials Engineering, Ben-Gurion University of the Negev, Beer-Sheva 84105, Israel; orcid.org/0000-0003-4902-1980

Bapan Pramanik – Department of Chemistry, Ben-Gurion University of the Negev, Beer-Sheva 84105, Israel; orcid.org/0000-0002-8860-2975

Nathaniel Wagner – Department of Chemistry, Ben-Gurion University of the Negev, Beer-Sheva 84105, Israel

Rivka Cohen-Luria – Department of Chemistry, Ben-Gurion University of the Negev, Beer-Sheva 84105, Israel

Complete contact information is available at: <https://pubs.acs.org/10.1021/jacs.1c06356>

Author Contributions

C.G. and V.K. contributed equally to this work.

Notes

The authors declare no competing financial interest.

ACKNOWLEDGMENTS

This work was supported by The German Israeli Project Cooperation (DIP) under Grants AS 424/1-1 and TO 266/8-1 and by the KAMIN program #56279 of MOST-Israel. V.K. acknowledges the generous support of the BGU Kreitman School for postdoctorate fellowship. We are grateful to Prof. Robert Tampé and Prof. Marc Tornow for fruitful discussions.

REFERENCES

- (1) Huang, P.-S.; Boyken, S. E.; Baker, D. The Coming of Age of De Novo Protein Design. *Nature* **2016**, *537*, 320–327.
- (2) Baker, E. G.; Bartlett, G. J.; Porter Goff, K. L.; Woolfson, D. N. Miniprotein Design: Past, Present, and Prospects. *Acc. Chem. Res.* **2017**, *50*, 2085–2092.
- (3) Amit, M.; Yuran, S.; Gazit, E.; Reches, M.; Ashkenasy, N. Tailor-Made Functional Peptide Self-Assembling Nanostructures. *Adv. Mater.* **2018**, *30*, 1707083.
- (4) Merg, A. D.; van Genderen, E.; Bazrafshan, A.; Su, H.; Zuo, X.; Touponse, G.; Blum, T. B.; Salaita, K.; Abrahams, J. P.; Conticello, V. P. Seeded Heteroepitaxial Growth of Crystallizable Collagen Triple Helices: Engineering Multifunctional Two-Dimensional Core-Shell Nanostructures. *J. Am. Chem. Soc.* **2019**, *141*, 20107–20117.
- (5) Pappas, C. G.; Shafi, R.; Sasselli, I. R.; Siccardi, H.; Wang, T.; Narang, V.; Abzalimov, R.; Wijerathne, N.; Ulijn, R. V. Dynamic Peptide Libraries for the Discovery of Supramolecular Nanomaterials. *Nat. Nanotechnol.* **2016**, *11*, 960–967.
- (6) Ivnitiski, D.; Amit, M.; Silberbush, O.; Atsmon-Raz, Y.; Nanda, J.; Cohen-Luria, R.; Miller, Y.; Ashkenasy, G.; Ashkenasy, N. The Strong

Influence of Structure Polymorphism on the Conductivity of Peptide Fibrils. *Angew. Chem., Int. Ed.* **2016**, *55*, 9988–9992.

(7) Bai, Y.; Chotera, A.; Taran, O.; Liang, C.; Ashkenasy, G.; Lynn, D. G. Achieving Biopolymer Synergy in Systems Chemistry. *Chem. Soc. Rev.* **2018**, *47*, 5444–5456.

(8) Sola, J.; Jimeno, C.; Alfonso, I. Exploiting Complexity to Implement Function in Chemical Systems. *Chem. Commun.* **2020**, *56*, 13273–13286.

(9) Lampel, A. Biology-Inspired Supramolecular Peptide Systems. *Chem.* **2020**, *6*, 1222–1236.

(10) Ashkenasy, G.; Hermans, T. M.; Otto, S.; Taylor, A. F. Systems Chemistry. *Chem. Soc. Rev.* **2017**, *46*, 2543–2554.

(11) Chen, C.; Tan, J.; Hsieh, M.-C.; Pan, T.; Goodwin, J. T.; Mehta, A. K.; Grover, M. A.; Lynn, D. G. Design of Multi-Phase Dynamic Chemical Networks. *Nat. Chem.* **2017**, *9*, 799–804.

(12) Bharat, T. A. M.; von Kugelgen, A.; Alva, V. Molecular Logic of Prokaryotic Surface Layer Structures. *Trends Microbiol.* **2021**, *29*, 405–415.

(13) Geoghegan, J. A.; Foster, T. J. Cell Wall-Anchored Surface Proteins of *Staphylococcus Aureus*: Many Proteins, Multiple Functions. *Curr. Top. Microbiol. Immunol.* **2015**, *409*, 95–120.

(14) Gerbino, E.; Carasi, P.; Mobili, P.; Serradell, M. A.; Gomez-Zavaglia, A. Role of S-Layer Proteins in Bacteria. *World J. Microbiol. Biotechnol.* **2015**, *31*, 1877–1887.

(15) Missiakas, D.; Schneewind, O. Assembly and Function of the *Bacillus Anthracis* S-Layer. *Annu. Rev. Microbiol.* **2017**, *71*, 79–98.

(16) Zhu, C.; Guo, G.; Ma, Q.; Zhang, F.; Ma, F.; Liu, J.; Xiao, D.; Yang, X.; Sun, M. Diversity in S-Layers. *Prog. Biophys. Mol. Biol.* **2017**, *123*, 1–15.

(17) Katz, E. Enzyme-Based Logic Gates and Networks with Output Signals Analyzed by Various Methods. *ChemPhysChem* **2017**, *18*, 1688–1713.

(18) Katz, E. Boolean Logic Gates Realized with Enzyme-Catalyzed Reactions - Unusual Look at Usual Chemical Reactions. *ChemPhysChem* **2019**, *20*, 9–22.

(19) Wagner, N.; Ashkenasy, G. Systems Chemistry: Logic Gates, Arithmetic Units and Network Motifs in Small Networks. *Chem. - Eur. J.* **2009**, *15*, 1765–1775.

(20) Ashkenasy, G.; Dadon, Z.; Alesebi, S.; Wagner, N.; Ashkenasy, N. Building Logic into Peptide Networks: Bottom-up and Top-Down. *Isr. J. Chem.* **2011**, *51*, 106–117.

(21) Holt, B. A.; Kwong, G. A. Protease Circuits for Processing Biological Information. *Nat. Commun.* **2020**, *11*, 5021.

(22) Angerani, S.; Winssinger, N. Sense-and-Release Logic-Gated Molecular Network Responding to Dimeric Cell Surface Proteins. *J. Am. Chem. Soc.* **2020**, *142*, 12333–12340.

(23) Claussen, J. C.; Hildebrandt, N.; Susumu, K.; Ancona, M. G.; Medintz, I. L. Complex Logic Functions Implemented with Quantum Dot Bionanophotonic Circuits. *ACS Appl. Mater. Interfaces* **2014**, *6*, 3771–3778.

(24) Li, Y.; Sun, S.; Fan, L.; Hu, S.; Huang, Y.; Zhang, K.; Nie, Z.; Yao, S. Peptide Logic Circuits Based on Chemoenzymatic Ligation for Programmable Cell Apoptosis. *Angew. Chem., Int. Ed.* **2017**, *56*, 14888–14892.

(25) de Ruiter, G.; van der Boom, M. E. Surface-Confined Assemblies and Polymers for Molecular Logic. *Acc. Chem. Res.* **2011**, *44*, 563–573.

(26) Ling, J.; Daly, B.; Silversen, V. A. D.; de Silva, A. P. Taking Baby Steps in Molecular Logic-Based Computation. *Chem. Commun.* **2015**, *51*, 8403–8409.

(27) Andreasson, J.; Pischel, U. Molecules with a Sense of Logic: A Progress Report. *Chem. Soc. Rev.* **2015**, *44*, 1053–1069.

(28) Magri, D. C. Logical Sensing with Fluorescent Molecular Logic Gates Based on Photoinduced Electron Transfer. *Coord. Chem. Rev.* **2021**, *426*, 213598.

(29) Deng, H.-H.; Wang, F.-F.; Liu, Y.-H.; Peng, H.-P.; Li, K.-L.; Liu, A.-L.; Xia, X.-H.; Chen, W. Label-Free, Resettable, and Multi-Readout Logic Gates Based on Chemically Induced Fluorescence

Switching of Gold Nanoclusters. *J. Mater. Chem. C* **2016**, *4*, 7141–7147.

(30) Gdor, E.; Katz, E.; Mandler, D. Biomolecular and Logic Gate Based on Immobilized Enzymes with Precise Spatial Separation Controlled by Scanning Electrochemical Microscopy. *J. Phys. Chem. B* **2013**, *117*, 16058–16065.

(31) Mondal, P. C.; Singh, V.; Zharnikov, M. Nanometric Assembly of Functional Terpyridyl Complexes on Transparent and Conductive Oxide Substrates: Structure, Properties, and Applications. *Acc. Chem. Res.* **2017**, *50*, 2128–2138.

(32) Jiang, Y.; Liu, N.; Guo, W.; Xia, F.; Jiang, L. Highly-Efficient Gating of Solid-State Nanochannels by DNA Supersandwich Structure Containing Atp Aptamers: A Nanofluidic Implication Logic Device. *J. Am. Chem. Soc.* **2012**, *134*, 15395–15401.

(33) Harbury, P. B.; Zhang, T.; Kim, P. S.; Alber, T. A Switch between Two-, Three-, and Four-Stranded Coiled Coils in Gcn4 Leucine Zipper Mutants. *Science* **1993**, *262*, 1401–1407.

(34) Hill, R. B.; Raleigh, D. P.; Lombardi, A.; DeGrado, W. F. De Novo Design of Helical Bundles as Models for Understanding Protein Folding and Function. *Acc. Chem. Res.* **2000**, *33*, 745–754.

(35) Woolfson, D. N. The Design of Coiled-Coil Structures and Assemblies. *Adv. Protein Chem.* **2005**, *70*, 79–112.

(36) Oakley, M. G.; Hollenbeck, J. J. The Design of Antiparallel Coiled Coils. *Curr. Opin. Struct. Biol.* **2001**, *11*, 450–7.

(37) Ashkenasy, G.; Ghadiri, M. R. Boolean Logic Functions of a Synthetic Peptide Network. *J. Am. Chem. Soc.* **2004**, *126*, 11140–11141.

(38) Dadon, Z.; Samiappan, M.; Safranchik, E. Y.; Ashkenasy, G. Light-Induced Peptide Replication Controls Logic Operations in Small Networks. *Chem. - Eur. J.* **2010**, *16*, 12096–12099.

(39) Samiappan, M.; Dadon, Z.; Ashkenasy, G. Replication Nand Gate with Light as Input and Output. *Chem. Commun.* **2011**, *47*, 710–712.

(40) Atkinson, J. T.; Campbell, I. J.; Thomas, E. E.; Bonitatibus, S. C.; Elliott, S. J.; Bennett, G. N.; Silberg, J. J. Metalloprotein Switches That Display Chemical-Dependent Electron Transfer in Cells. *Nat. Chem. Biol.* **2019**, *15*, 189–195.

(41) Fink, T.; Lonžarić, J.; Praznik, A.; Plaper, T.; Merljak, E.; Leben, K.; Jerala, N.; Lebar, T.; Strmšek, Z.; Lapenta, F.; Bencina, M.; Jerala, R. Design of Fast Proteolysis-Based Signaling and Logic Circuits in Mammalian Cells. *Nat. Chem. Biol.* **2019**, *15*, 115–122.

(42) Gao, X. J.; Chong, L. S.; Kim, M. S.; Elowitz, M. B. Programmable Protein Circuits in Living Cells. *Science* **2018**, *361*, 1252–1258.

(43) Chen, Z. De Novo Design of Protein Logic Gates. *Science* **2020**, *368*, 78.

(44) Shlizerman, C.; Atanassov, A.; Berkovich, I.; Ashkenasy, G.; Ashkenasy, N. De Novo Designed Coiled-Coil Proteins with Variable Conformations as Components of Molecular Electronic Devices. *J. Am. Chem. Soc.* **2010**, *132*, 5070–5076.

(45) White, S. J.; Morton, D. W. A.; Cheah, B. C.; Bronowska, A.; Davies, A. G.; Stockley, P. G.; Walti, C.; Johnson, S. On-Surface Assembly of Coiled-Coil Heterodimers. *Langmuir* **2012**, *28*, 13877–13882.

(46) Minelli, C.; Liew, J. X.; Muthu, M.; Andresen, H. Coiled Coil Peptide-Functionalized Surfaces for Reversible Molecular Binding. *Soft Matter* **2013**, *9*, 5119–5124.

(47) Stevens, M. M.; Flynn, N. T.; Wang, C.; Tirrell, D. A.; Langer, R. Coiled-Coil Peptide-Based Assembly of Gold Nanoparticles. *Adv. Mater.* **2004**, *16*, 915–918.

(48) Siehr, A.; Xu, B.; Siegel, R. A.; Shen, W. Colloidal Stability Versus Self-Assembly of Nanoparticles Controlled by Coiled-Coil Protein Interactions. *Soft Matter* **2019**, *15*, 7122–7126.

(49) Ding, D.; Gao, P.; Ma, Q.; Wang, D.; Xia, F. Biomolecule-Functionalized Solid-State Ion Nanochannels/Nanopores: Features and Techniques. *Small* **2019**, *15*, 1804878.

(50) Long, Z.; Zhan, S.; Gao, P.; Wang, Y.; Lou, X.; Xia, F. Recent Advances in Solid Nanopore/Channel Analysis. *Anal. Chem.* **2018**, *90*, 577–588.

(51) Perez-Mitta, G.; Toimil-Molares, M. E.; Trautmann, C.; Marmisolle, W. A.; Azzaroni, O. Molecular Design of Solid-State Nanopores: Fundamental Concepts and Applications. *Adv. Mater.* **2019**, *31*, 1901483.

(52) Horne, W. S.; Yadav, M. K.; Stout, C. D.; Ghadiri, M. R. Heterocyclic Peptide Backbone Modifications in an A-Helical Coiled Coil. *J. Am. Chem. Soc.* **2004**, *126*, 15366–15367.

(53) Oshaben, K. M.; Salari, R.; McCaslin, D. R.; Chong, L. T.; Horne, W. S. The Native Gcn4 Leucine-Zipper Domain Does Not Uniquely Specify a Dimeric Oligomerization State. *Biochemistry* **2012**, *51*, 9581–9591.

(54) Xu, C.; Liu, R.; Mehta, A. K.; Guerrero-Ferreira, R. C.; Wright, E. R.; Dunin-Horkawicz, S.; Morris, K.; Serpell, L. C.; Zuo, X.; Wall, J. S.; Conticello, V. P. Rational Design of Helical Nanotubes from Self-Assembly of Coiled-Coil Lock Washers. *J. Am. Chem. Soc.* **2013**, *135*, 15565–15578.

(55) Gradisar, H.; Bozic, S.; Doles, T.; Vengust, D.; Hafner-Bratkovic, I.; Mertelj, A.; Webb, B.; Sali, A.; Klavzar, S.; Jerala, R. Design of a Single-Chain Polypeptide Tetrahedron Assembled from Coiled-Coil Segments. *Nat. Chem. Biol.* **2013**, *9*, 362–366.

(56) Chen, Z.; Boyken, S. E.; Jia, M.; Busch, F.; Flores-Solis, D.; Bick, M. J.; Lu, P.; VanAernum, Z. L.; Sahasrabudhe, A.; Langan, R. A.; Bermeo, S.; Brunette, T. J.; Mulligan, V. K.; Carter, L. P.; DiMaio, F.; Sgourakis, N. G.; Wysocki, V. H.; Baker, D. Programmable Design of Orthogonal Protein Heterodimers. *Nature* **2019**, *565*, 106–111.

(57) Marsden, H. R.; Tomatsu, I.; Kros, A. Model Systems for Membrane Fusion. *Chem. Soc. Rev.* **2011**, *40*, 1572–1585.

(58) Merg, A. D.; Touponse, G.; van Genderen, E.; Zuo, X.; Bazrafshan, A.; Blum, T.; Hughes, S.; Salaita, K.; Abrahams, J. P.; Conticello, V. P. 2d Crystal Engineering of Nanosheets Assembled from Helical Peptide Building Blocks. *Angew. Chem., Int. Ed.* **2019**, *58*, 13507–13512.

(59) Dadon, Z.; Samiappan, M.; Shahar, A.; Zarivach, R.; Ashkenasy, G. A High-Resolution Structure That Provides Insight into Coiled-Coil Thiodipeptide Dynamic Chemistry. *Angew. Chem., Int. Ed.* **2013**, *52*, 9944–9947.

(60) Lee, K.; Park, K.-B.; Kim, H.-J.; Yu, J.-S.; Chae, H.; Kim, H.-M.; Kim, K.-B. Recent Progress in Solid-State Nanopores. *Adv. Mater.* **2018**, *30*, 1704680.

(61) Liu, L.; Wu, H.-C. DNA-Based Nanopore Sensing. *Angew. Chem., Int. Ed.* **2016**, *55*, 15216–15222.

(62) Shi, W.; Friedman, A. K.; Baker, L. A. Nanopore Sensing. *Anal. Chem.* **2017**, *89*, 157–188.

(63) Liebes-Peer, Y.; Rapaport, H.; Ashkenasy, N. Amplification of Single Molecule Translocation Signal Using B-Strand Peptide Functionalized Nanopores. *ACS Nano* **2014**, *8*, 6822–6832.

(64) Kowalczyk, S. W.; Grosberg, A. Y.; Rabin, Y.; Dekker, C. Modeling the Conductance and DNA Blockade of Solid-State Nanopores. *Nanotechnology* **2011**, *22*, 315101.

(65) Kaniewska, K.; Bollella, P.; Katz, E. Implication and Inhibition Boolean Logic Gates Mimicked with Enzyme Reactions. *ChemPhysChem* **2020**, *21*, 2150–2154.

(66) Huang, K.; Szleifer, I. Design of Multifunctional Nanogate in Response to Multiple External Stimuli Using Amphiphilic Diblock Copolymer. *J. Am. Chem. Soc.* **2017**, *139*, 6422–6430.

(67) Watson, E. E.; Angerani, S.; Sabale, P. M.; Winssinger, N. Biosupramolecular Systems: Integrating Cues into Responses. *J. Am. Chem. Soc.* **2021**, *143*, 4467–4482.